

Analysis of Electronic Transport in a Single-Phonon Resonance mid-IR Quantum Cascade Laser

G. Hałdaś, A. Kolek

Department of Electronics Fundamentals
Rzeszów University of Technology
35-959 Rzeszów, Poland
ghaldas@prz.edu.pl, akoleknd@prz.edu.pl

D. Pierścińska, P. Gutowski, K. Pierściński,
P. Karbownik, M. Bugajski
Institute of Electron Technology
Al. Lotników 32/46, 02 668 Warszawa, Poland

Abstract—Non-equilibrium Green's function method is used to analyze electronic transport in a mid-infrared quantum cascade laser on microscopic level. Basing on the excellent agreement found between calculated and experimental data, the conclusions are derived that the carrier distribution in the lower laser subband is non-thermal, and the carriers are extracted from active region both in cold and hot state. An estimate 0.52 ps of upper lifetime was found which considerably differs from the value evaluated from the form factors.

Keywords—non-equilibrium Green's function, quantum cascade laser, electronic transport, optical gain.

I. INTRODUCTION

Quantum cascade lasers (QCLs) are one of the most sophisticated optoelectronic devices. Understanding their operation requires involving an advanced approach that takes into account both scattering and quantum coherence what can be achieved with Density Matrix (DM) or Non-Equilibrium Green's Function (NEGF) methods [1]. However, these methods are highly demanding, both conceptually and computationally, so their use in QCL modeling needs some simplifications. Consequently, the existing implementations of NEGF and DM use the basis cut to several quantum states per one QCL period [2], do not fully resolve for in-plane momentum [2,3], and limit the analysis to at most three device's modules [2-5]. They use effective mass Hamiltonians limited to at most two bands, so the effect of bands mixing is also simplified. In spite of this, the results offered by these methods are worth the price being paid: They agree well with the experimental data while only few parameters in the theoretical model are adjustable. This, almost "fit-free", agreement validates these methods and gives all calculated quantities, including those which are experimentally inaccessible, the status of reliable estimates of the real quantities. In many cases, having such a response is crucial for the verification of the designing assumptions and better understanding of device operation. One of such quantities that could serve as an example is an energetic spectrum of the carriers crossing injection or extraction barriers which are believed to be fully thermalized but, as shown in the following, can be quite different.

Obviously, the quality of the mentioned estimates depends on the number of the simplifications used in the theoretical

The work was supported by the Poland Ministry of Science and Education Funds for statutory activity (DS) through Rzeszów University of Technology Grant no U-596/DS (GH and AK) and the National Science Center (NCN), under the projects SONATA 2013/09/D/ST7/03966 (DP and KP) and PRELUDIUM 2015/17/N/ST7/03936 (PG.).

(numerical) model. While most of those listed above can be easily released for THz devices, only few works report on the modeling of mid-IR QCLs with DM/NEGF that are fully energy and (in-plane) momentum resolved, account for band mixing, and use non-cut basis [5,6]. This paper adds to these by presenting the analysis of the electronic transport and optical gain with the NEGF model applied to the mid-IR QCL emitting at $\sim 9 \mu\text{m}$ that uses a single-phonon resonance scheme of lower subband depopulation.

II. THE MODEL

QCLs are purely unipolar, n-type devices, so the model uses a single-band effective mass Hamiltonian. Mixing with the valence bands is taken into account, making electron effective mass, m energy (E) dependent. Namely, $m(E, z) = m^*(z)\{1 + [E - E_c(z)]/E_g(z)\}$, where $E_c(z)$ and $E_g(z)$ are the conduction band edge and band gap respectively, and z is the growth direction. The in-plane dynamics is included by kinetic energy terms with isotropic, still energy-dependent, effective mass. Such a choice preserves the in-plane non-parabolicity, comparable to the results predicted by 8-band kp method [7]. The full non-interacting Hamiltonian reads

$$H = \frac{-\hbar^2}{2} \frac{d}{dz} \frac{1}{m(E, z)} \frac{d}{dz} + V(z) + \frac{\hbar^2 k^2}{m(E, z)}, \quad (1)$$

where the potential energy term $V(z)$ comprises the conduction band edge offsets $E_c(z)$, the external bias U , and the Hartree term calculated self-consistently by the solution of the Poisson equation. Calculations are made in the real space. The Hamiltonian (1) is discretized and the grid points define its base vectors. This basis is quite large as the mesh of 76 grid points is used to map the QCL structure. The formulations for scattering self-energies in this basis were provided in refs. [1,4] and [8]. For the alloy disorder, LO-phonon, the interface roughness (IR) and the ionized impurity scatterings we use the formulations of ref. [8] whereas for the acoustic (LA) phonons we use energy-averaged approximation of ref. [4]. Unlike others, the NEGF method does not *a-priori* assume that carriers within the QCL subbands are thermalized. Just the opposite, the intrasubband carriers distributions are calculated self-consistently. Accordingly, there is no need to introduce some electronic temperature and the only temperature in the model is the ambient (lattice) temperature, T . The mentioned size of the

basis refers to the central period of QCL device. The remaining parts are imitated by the left and right hand contact (retarded) self-energies $\Sigma_{L,R}$. They were calculated by solving the Dyson equation for the QCL periods connected to the central one on its left (L) or right (R) hand side. The boundary conditions used in the calculations of $\Sigma_{L,R}$ assume that L/R period is connected to the semi-infinite, homogeneous leads on its left/right side and the hard wall on its right/left side. Scattering within the L/R period was included in the simplified manner by introducing dephasing, momentum relaxing (diagonal) self-energies [4].

In the real space basis representation, the Green's functions G^R , $G^<$, are the four-parameter functions of positions z , z' , the in-plane momentum modulus k , and the energy E . They can be found by an iterative solution of the Dyson, Keldysh, and Poisson equation. Then, the energy, momentum and position resolved densities of states (DOS), electrons (DOE) and current (J) can be found through well-known relations connecting these quantities with $G^{R,<}(E, k, z, z')$ [1,4,8].

III. RESULTS

Our NEGF-based solver was used to simulate electronic transport and optical gain in the mid-IR GaAs QCL design of ref. [9]. Most of the parameters in the formulations of scattering self-energies are material or temperature dependent. In fact the only parameters that are unknown and can be treated as adjustable are interface roughness rms height Δ and correlation radius Λ . The adjustment can be done by fitting calculated and experimental I-V curves and threshold currents. Data in Fig. 1 show results of such fitting. Structures for the comparison were grown and processed into real devices and for this study the samples were selected which give overlapped I-V curves for different waveguide cross-sections what ensures that leakage currents are minimized. The values $\Delta = 0.19$ nm and $\Lambda = 9$ nm used for best fitting are quite reliable if compared to the independent estimates of these parameters reported in the literature. Reasonable choice of the Δ and Λ values is further confirmed by the results of the calculations shown in Fig. 2. Namely, the calculated gain spectrum $g(h\nu)$, which peaks at $h\nu = 0.127$ meV corresponding very close to the experimental wavelength of $\lambda = 9.6$ μm , has the FWHM of 13 meV in close agreement with the measured FWHM = 12 meV of electroluminescence [9].

The results of the simulations are shown in Figs. 2 and 3. The energy-momentum resolved electronic densities calculated for the external bias $U = 192$ mV/period (overall voltage is 36 (cascade no.) $\times U = 6.91$ V) are shown in Fig. 2. The distributions of the currents crossing injection or extraction barrier a in E - k^2 space are shown in Fig. 3. With such data, the detailed and in-depth analysis of the electronic transport in QCL can be made. Example conclusions derived from Figs. 2 and 3 are that the population inversion is observed for the applied bias what results in optical gain. However, the carriers in the lower laser subband (no. 2) are not fully thermalized, and they are able to leave the active region in this non-thermalized state. Another analysis that can be easily performed concerns the upper state lifetime τ_3 which is an important QCL parameter. It can be found from the relation $J = en_3/\tau_3$ plotting the upper state population n_3 versus the current density J (Fig. 3 inset). The lifetime $\tau_3 = 0.52$ ps we get, is significantly shorter the value $\tau_3 = 1.4$ ps calculated from the form factors and assumed in the designing process [9]. In spite of this, it is possible to get inversion due to the non-thermal occupation of

the lower subband since the low- k states, which otherwise are more populated, mainly contribute to the optical gain.

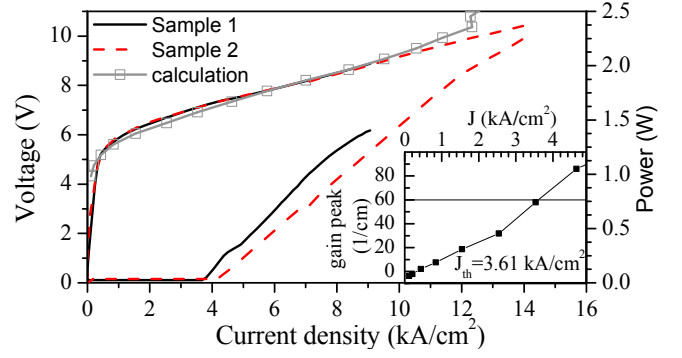


Fig. 1. Experimental (lines) and calculated (lines and symbols) current-voltage-light characteristics at the temperature $T = 77$ K. Inset: calculated gain peak versus current density compared to the overall losses divided by the confinement factor $(\alpha_w + \alpha_m)/T = 60$ cm^{-1} .

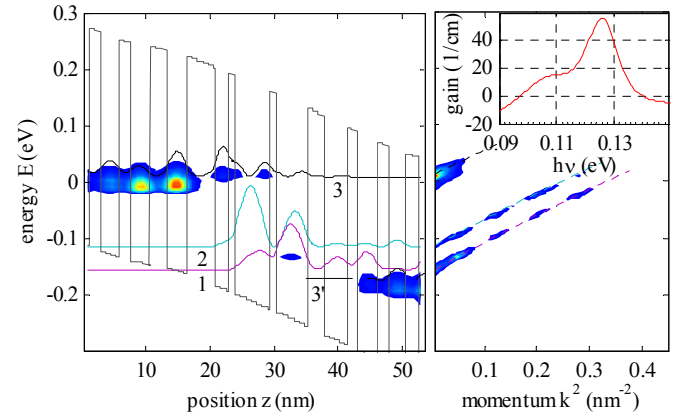


Fig. 2. (left) Conduction band profile, laser (3, 2) and depopulating (1) levels wavefunctions (modulus squared) and electron density (contour color plot). (right) In-plane momentum resolved electron density in subbands 1-3. (inset) Gain spectrum, all calculated with the NEGF method.

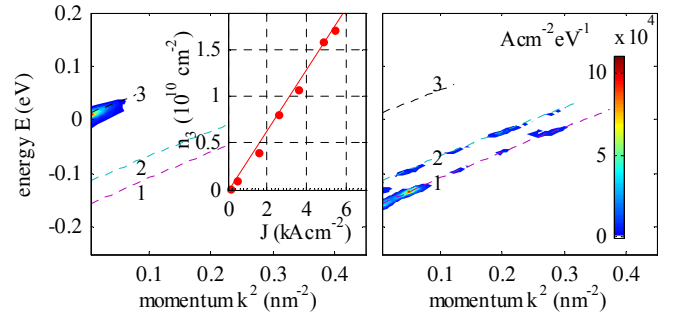


Fig. 3. The energy-momentum resolved density of current at (left) $z = 18$ nm (right) $z = 37$ nm calculated for the structure and the bias like in Fig. 2. (inset) Upper state population n_3 versus current density J .

REFERENCES

- [1] C. Jirauschek and T. Kubis, *Appl. Phys. Rev.* **1** 011307, 2014.
- [2] S.-C. Lee and A. Wacker, *Phys. Rev. B* **66** 245314, 2002.
- [3] R. Terazzi and J. Faist, *New J. Phys.* **12** 033045, 2010.
- [4] JT. Kubis, C. Yeh, and P. Vogl, *Phys. Rev. B* **79** 195323, 2009.
- [5] G. Haldáš, A. Kolek, I. Tralle, *IEEE J. Quantum Electron.* **47** 78, 2011.
- [6] A. Kolek, G. Haldáš, M. Bugajski, *Appl. Phys. Lett.* **101** 161110, 2012.
- [7] J. Faist, *Quantum Cascade Lasers*, Oxford Univ. Press, Oxford, 2013.
- [8] R. Lake, et al *J. Appl. Phys.* **81** 7845, 1998.
- [9] H. Page et al *Appl. Phys. Lett.* **78** 3529, 2001.